Onsets of Tethered Chain Overcrowding and Highly Stretched Brush Regime via Crystalline−Amorphous Diblock Copolymers

Joseph X. Zheng,[†] Huiming Xiong,[†] William Y. Chen,[†] Kyungmin Lee,[†] Ryan M. Van Horn,[†] Roderic P. Quirk,[†] Bernard Lotz,[‡] Edwin L. Thomas,[§] An-Chang Shi,[⊥] and Stephen Z. D. Cheng*[,†]

Maurice Morton Institute and Department of Polymer Science, The University of Akron, Akron, Ohio 44328-3909; Institut of Charles Sadron, 6 Rue Boussingault, Strasbourg 67083, France; Department of Materials Science and Engineering, Massachusetts Institute of Technology, Cambridge, Massachusetts 02139; and Department of Physics and Astronomy, McMaster University, Hamilton, Ontario L8S 4M1, Canada

Received October 6, 2005; Revised Manuscript Received November 22, 2005

ABSTRACT: Lamellar single crystals grown in dilute solutions can be used as templates for tethered chain analysis. Two series of diblock copolymers, poly(ethylene oxide)-*block*-polystyrene (PEO-*b*-PS) and poly(L-lactic acid)-*block*-polystyrene (PLLA-*b*-PS), were used as model templates to generate tethered PS blocks on the single-crystal basal surfaces. Controlled and tunable reduced tethering density, $\tilde{\sigma}$, defined by $\sigma\pi R_g^2$ (where σ is the tethered chain density and is equal to the reciprocal of the covered area of the chain and R_g is the radius of gyration of this tethered chain in its end-free state at the same conditions), could be achieved in a broad range (up to 24) by changing the molecular weights (MW's) of the crystalline and amorphous blocks and by varying the crystallization temperature (T_x) of different PEO-*b*-PS and PLLA-*b*-PS solutions. For PEO and PLLA homopolymers crystallized in dilute solutions, the lamellar crystal thicknesses (d_{CRYST}) were observed to be proportional to the reciprocal undercooling ΔT (where $\Delta T = T_d - T_x$ and T_d is the equilibrium dissolution temperature of the crystals). The $\tilde{\sigma}$ of the tethered PS chains on the crystal surface increased with decreasing ΔT because at a fixed MW of the PEO or PLLA block, an increase in the d_{CRYST} was evidence of a decrease in the number of folds. When we plotted the relationships between $1/d_{CRYST}$ and T_x for these two series of diblock copolymers, sudden and discontinuous changes of the slopes in some of these were observed at $\tilde{\sigma} = 3.7$ ($\tilde{\sigma}$*). This was as a result of the drastic interaction change of the neighboring PS tethered chains. An average reduced surface free energy of the tethered PS chains (Γ^{PS}) was defined and used as a parameter to characterize the PS tethered chain interactions. The relationship between Γ^{PS} and $\tilde{\sigma}$ showed a discontinuous transition at $\tilde{\sigma}$*, which had a close similarity to the hard-sphere-like interaction model. This could be identified as the onset of the tethered PS chain overcrowding in solution. This transition indicates that the extra entropic surface free energy created by the repulsion of tethered PS chains started to affect the nucleation barrier of the PEO or PLLA block crystallization. On the basis of the scaling laws, the onset of highly stretched brush regime could be identified at $\tilde{\sigma} = 14.3$ ($\tilde{\sigma}$**). In the Γ^{PS} vs $\tilde{\sigma}$ plot, the transition appears to be continuous. Thus, a crossover regime in the tethered PS chains exists between $\tilde{\sigma}^* = 3.7$ and $\tilde{\sigma}^{**} = 14.3$. It is defined as the regime where the interaction of the tethered PS chains undergoes changes from being noninteracting toward penetration to, finally, chain stretching normal to the surface.

Introduction

Crystalline−amorphous diblock copolymers have been widely used as templates to construct nanophase structures in investigations of polymer phase structures and their transformations in multiple length scales. The majority of the work in the past 15 years has been focused on the diblock copolymers in the bulk state.[1−14] It has also been known for about 40 years that the crystalline−amorphous diblock copolymers, in particular poly(ethylene oxide)-*block*-polystyrene (PEO-*b*-PS) copolymers, can grow single crystals in dilute solutions. It was reported that the single crystals have a "sandwiched" structure with the PEO single crystal in the middle covered by two nano-PS block layers on the top and bottom of the PEO basal surface.[15−17] The PS blocks at the surface of the PEO block single crystals can be viewed as tethered chains on a substrate. We have developed an approach to study interactions of tethered PS chains on a single-crystal substrate with controlled and uniform tethering densities. We utilized the single-crystal thickness (d_{CRYST}) grown in different solutions as a probe to monitor changes with respect to the crystallization temperature (T_x). The d_{CRYST} is sensitive to the extra surface free energy generated by the tethered PS chains when they experience repulsive interactions with each other.[18]

Direct and precise thickness determinations of the tethered amorphous chains, d_{AM} and d_{CRYST}, are difficult in solution; however, after a single crystal is dried, the d_{CRYST} is identical to that in solution. An overall thickness of a crystalline−amorphous block copolymer single crystal ($d_{OVERALL}$) after drying can be measured using atomic force microscopy (AFM). It includes three layers: a lamellar single-crystal layer covered by two amorphous block layers on both sides or a "sandwiched" structure.[15−18] To calculate the d_{CRYST} and the d_{AM} values based on the $d_{OVERALL}$ data, we need to know volume fractions of the crystalline and amorphous blocks. On the basis of the molecular weights (MW's) and densities of the blocks in the solid state, the d_{CRYST} and d_{AM} thicknesses can be estimated using the

[†] The University of Akron.
[‡] Institut of Charles Sadron.
[§] Massachusetts Institute of Technology.
[⊥] McMaster University.
* To whom correspondence should be addressed: e-mail scheng@uakron.edu.

10.1021/ma052166w CCC: $33.50
Published on Web 12/30/2005

following approximations:[18]

$$d_{CRYST} = d_{OVERALL} v_{CRYST}$$

$$v_{CRYST} = \frac{M_n^{CRYST}/\rho_{CRYST}}{M_n^{CRYST}/\rho_{CRYST} + M_n^{AM}/\rho_{AM}} \quad (1a)$$

and

$$d_{AM} = \frac{d_{OVERALL} v_{AM}}{2}$$

$$v_{AM} = \frac{M_n^{AM}/\rho_{AM}}{M_n^{CRYST}/\rho_{CRYST} + M_n^{AM}/\rho_{AM}} \quad (1b)$$

where M_n^{CRYST} and M_n^{AM} are the MW's of the crystallizable and amorphous blocks, ρ_{CRYST} and ρ_{AM} are densities of the crystalline and amorphous blocks, respectively, and ν_{CRYST} and ν_{AM} represent volume fractions of crystallizable and amorphous blocks. Since polymer crystals do not reach 100% crystallinity, the ρ_{CRYST} has to be further considered as a combination of both the crystalline and the amorphous parts of the crystallizable blocks (the two-phase model). Therefore, the crystallinity (w^c) and the crystalline and amorphous densities of the crystallizable block (ρ^a_{CRYST} and ρ^c_{CRYST}) are necessary parameters. The ρ_{CRYST} value is thus

$$\rho_{CRYST} = \rho^c_{CRYST} w^c + \rho^a_{CRYST}(1 - w^c) \quad (1c)$$

On the other hand, the density of the tethered chains at a surface, σ, which describes how close the neighboring tethered chains are located, is defined to be the reciprocal average covering area of each chain, S. Therefore, the physical meaning of tethering density is the number of tethered chains in a unit area surface.[19−23] For a crystalline−amorphous diblock copolymer, when the amorphous blocks are tethered onto single-crystal surfaces of the crystalline blocks, S and σ can be calculated by

$$\sigma = 1/S = 1/\left(\frac{2M_n^{CRYST}}{N_A \rho_{CRYST} d_{CRYST}}\right) = \frac{N_A \rho_{CRYST} d_{CRYST}}{2M_n^{CRYST}} \quad (2)$$

where N_A is Avogadro's number. The factor 2 comes from the fact that each lamellar single crystal has two folded surfaces. Under thermodynamic equilibrium consideration, 50% of the amorphous chains are located on each of the two single-crystal surfaces when formed in solution. The thickness of the crystal is needed because it is a measure of the number of chain folds. This number is important in determining the number of tethering points. Theoretical treatment of single crystals of crystalline−amorphous diblock copolymers was first proposed by DiMarzio et al.[24]

In the past few decades, several approaches in forming tethered chain molecules on substrates have been utilized. They are physical adsorption[25,26] or chemically grafting chains onto substrates via the "grafting to" method[27,28] or "grafting from" polymerizations.[29−32] All these approaches have advantages along with specific issues that must be addressed. In particular, physical adsorption may not generate high enough σ values to reach the highly stretched brush regime, while the two chemical approaches may have less precise control over the uniformity of σ or the uniformity in controlling MW's of the tethered chains.

Advancements in theoretical developments of tethered chains on flat solid substrates have been achieved for the different brush regimes. The "noninteraction" regime and the "highly stretched brush" regime, particularly, are the primary focus. It has also been reported that the transition between these two regimes is rather broad, allowing a "crossover" regime to exist. In the theoretical treatments, of which the interaction between tethered chains and substrates is ignored (no favorable interaction exists), the quantity σ has been frequently used to describe how close a tethered chain is with its neighbors. The reduced tethering density ($\tilde{\sigma}$), proposed by Kent,[33] has been defined by $\tilde{\sigma} = \sigma\pi R_g^2$, where R_g is the radius of gyration of a tethered chain at its end-free state in the same conditions (i.e., solvent and temperature). This definition provides a parameter that is independent of the MW of tethered chains and the type of solvent used. In the noninteraction regime, the tethered chain behavior has been approximated by renormalization group theory.[34] When entering the crossover regime, the "single-chain mean-field theory" was used to describe the interactions.[35−37] The highly stretched brush regime has been treated with scaling laws,[38−42] numerical, self-consistent-field theory,[43−46] and Monte Carlo simulations.[47−49]

In the experimental aspects, most results reported were in the noninteraction and crossover regimes. The observations invoked the layer thickness measurements of the tethered chains in solution. Since the transition between the noninteraction and crossover regimes does not exhibit a significant increase of the layer thickness, it is qualitatively understood that the tethered chain crowding may happen around $\tilde{\sigma} = 1-3$. Kent's study showed that the strongly stretched brush regime was not reached even at a value of $\tilde{\sigma} \sim 12$.[33] On the other hand, another study reported that tethered chains started to be stretched at an estimated $\tilde{\sigma} \sim 6$, but the sample employed had a broad MW distribution (PDI = 1.7),[50] which likely affects the results. So the issue remains, where are the onsets of the tethered chain overcrowding and highly stretched brush regimes?

In this publication, using two series of crystalline−amorphous diblock copolymers, PEO-*b*-PS and poly(L-lactic acid)-*block*-polystyrene (PLLA-*b*-PS), we report our experimentally measured and calculated d_{CRYST} values and use them as the probes to quantitatively identify the onsets of tethered PS chain overcrowding and highly stretched PS brush regime via the investigation of how the d_{CRYST} values change under the influence of varying the tethered PS chain interactions on the crystal surfaces of the diblock copolymer single crystals.

Experimental Section

Materials Preparation. Two series of diblock copolymers, PEO-*b*-PS and PLLA-*b*-PS, were synthesized via the anionic polymerization of styrene followed by anionic polymerization of ethylene oxide or ring-opening polymerization of L-lactide. Detailed synthetic procedures can be found elsewhere.[51,52] The M_n^{PS} of the PS precursor was characterized by size exclusion chromatography (SEC) using polystyrene standards. The M_n^{PEO} and M_n^{PLLA} were determined based on the M_n^{PS} and proton nuclear magnetic resonance (^{1}H NMR), and the polydispersity in the final diblock copolymer was determined by SEC using universal calibration. The detailed molecular characterizations of these two series of diblock copolymers are listed in Tables 1 and 2. The PS bulk density (ρ_{PS}) is 1.052 g/cm^3, the crystalline PEO bulk density (ρ^c_{PEO}) is 1.239 g/cm^3, and the amorphous PEO bulk density (ρ^a_{PEO}) is 1.124 g/cm^3.[53] The value of the PLLA bulk density (ρ_{PLLA}) is less certain in the literature. It is known that the difference between the ρ^a_{PLLA} and ρ^c_{PLLA} is small near room temperature.[54] We measured the ρ_{PLLA} of homo-PLLA single crystals grown in amyl acetate dilute solution, and the $\rho_{PLLA} = 1.281 \pm 0.005$ g/cm^3, which is close to the reported value (1.275 g/cm^3).[55] It is also in good agreement with the average ρ^c_{PLLA}, 1.283 g/cm^3, of the α-form of PLLA

Table 1. Molecular Characterizations of Homo-PEO and PEO-*b*-PS Diblock Copolymers

sample ID	M_n^{PEO}(kg/mol)	M_n^{PS} (kg/mol)	$M_n^{OVERALL}$ (kg/mol)	PDI M_w/M_n	f_{PEO}
1. PEO	56.3	0	56.3	1.05	1.00
2. PEO-*b*-PS(17.0−3.0)	17.0	3.0	20.0	1.04	0.829
3. PEO-*b*-PS(11.0−4.6)	11.0	4.6	15.6	1.03	0.671
4. PEO-*b*-PS(40.1−7.7)	40.1	7.7	47.8	1.05	0.816
5. PEO-*b*-PS(23.0−5.0)	23.0	5.0	28.0	1.06	0.797
6. PEO-*b*-PS(16.7−5.0)	16.7	5.0	21.7	1.06	0.740
7. PEO-*b*-PS(20.3−6.8)	20.3	6.8	27.1	1.04	0.718
8. PEO-*b*-PS(9.4−6.7)	9.4	6.7	16.1	1.02	0.545
9. PEO-*b*-PS(8.7−9.2)	8.7	9.2	17.9	1.05	0.447
10. PEO-*b*-PS(11.0−17.0)	11.0	17.0	28.0	1.07	0.356

Table 2. Molecular Characterizations of Homo-PLLA and PLLA-*b*-PS Diblock Copolymers

sample ID	M_n^{PLLA} (kg/mol)	M_n^{PS} (kg/mol)	$M_n^{OVERALL}$ (kg/mol)	PDI M_w/M_n	f_{PLLA}
11. PLLA	12.9	0	12.9	1.24	1.00
12. PLLA-*b*-PS(27.3−6.0)	27.3	6.0	33.3	1.08	0.789
13. PLLA-*b*-PS(56.8−9.2)	56.8	9.2	66.0	1.14	0.835
14. PLLA-*b*-PS(31.8−9.2)	31.8	9.2	41.0	1.13	0.740
15. PLLA-*b*-PS(19.9−9.2)	19.9	9.2	29.1	1.07	0.640
16. PLLA-*b*-PS(15.0−9.2)	15.0	9.2	25.2	1.10	0.573
17. PLLA-*b*-PS(11.0−9.2)	11.0	9.2	20.2	1.04	0.496
18. PLLA-*b*-PS(18.0−19.3)	18.0	19.3	37.3	1.11	0.434

crystals calculated from the lattice parameters (1.253−1.303 g/cm^3, the range is due to different values of the lattice parameters).[55−58] Therefore, in this publication, $\rho_{PLLA} = 1.28$ g/cm^3 was used (with an error of less than 1%).

To measure R_g values of PS molecules, different MW's of PS homopolymers (between 3.0K and 20K g/mol) were polymerized via anionic polymerization. Both PEO and PLLA homopolymers ($M_n^{PEO} = 56.3$K g/mol, $M_n^{PLLA} = 12.9$K g/mol) were also synthesized to be references in growing single crystals to compare with those of the diblock copolymers.

Equipment and Experiments. A self-seeding technique was utilized to grow single crystals of all the samples listed in Tables 1 and 2. The detailed procedures were reported previously.[17] This procedure was used for single-crystal growth of the PEO homopolymer and PEO-*b*-PS diblock copolymers in both amyl acetate and a mixed solvent (chlorobenzene/octane, 1:1.1 weight ratio) and PLLA homopolymer and PLLA-*b*-PS diblock copolymers in amyl acetate. Note that the mixed solvent is close to the θ condition, while amyl acetate is a good solvent for PS blocks. In brief, e.g., the PLLA or PLLA-*b*-PS sample was added into amyl acetate with a concentration of 0.01 wt % and heated to 130 °C, which is above the dissolution temperature, in an oil bath with well-controlled temperature for 15 min to form a homogeneous solution. The solution was then left at room temperature overnight to allow the crystallization of the polymers. Subsequently, the sample was heated to the self-seeding temperature ($T_s = 110$ °C) in the oil bath for 15 min in order to dissolve most of the crystals, except for some small seeds (less than 1% of the crystals remained). The sample was then quickly switched into another isothermal oil bath with a preset T_x. Isothermal crystallization times of 4 h to 1 day were required to complete the single-crystal growth process depending on the T_x values.

A sequential crystallization of these two sets of diblock copolymers with PLLA or PEO homopolymer was also prepared by following the procedure as described in ref 17. After the complete crystallization of the diblock copolymer, a few drops of the samples containing the copolymer single-crystal seeds were added into the homogeneous solution of homopolymer which had been kept in the same crystallization oil bath. Note that the homogeneous homopolymer solution was prepared by heating the mixture of homopolymer and solvent at 0.01 wt % to 130 °C for 15 min. The solution was then quickly switched directly into the crystallization oil bath (at a preset T_x) for about 10 min to reach the thermal equilibrium before adding the diblock single-crystal seeds. During this 10 min period of time, no homopolymer crystals were found. The homopolymer then grew on the diblock copolymer single-crystal seeds to form composite single crystals.

For the AFM and TEM sample preparations, a few drops of the solution containing single crystals were placed onto carbon-coated cover glasses and washed with pure amyl acetate several times. The samples were subsequently dried in a vacuum oven at room temperature for 3 days to evaporate the solvent. The single crystals were then directly used for AFM experiments or transferred onto the copper grid for TEM observations.

Both the bright field (BF) images and the selective area electron diffraction (SAED) patterns of the single crystals were carried out in a JEOL (1200 EX II) TEM at an accelerating voltage of 120 kV. Calibration of the ED spacing was done using TlCl *d* spacing and their higher order diffractions. An AFM (Digital Instrument Nanoscope IIIA) was utilized to measure the lamellar thickness and the surface topology of the single crystals. The tapping mode was used in order to limit damage to the samples. The scanner was calibrated in both lateral and vertical directions using the standard grid. A typical measurement condition was at a scan size of 10 μm, a scan rate of 1 Hz, operation and resonance frequencies of 300 kHz, and a resolution of 512 × 512.

Results and Discussion

Lamellar Thicknesses of Homopolymer and Copolymer Single Crystals. Parts a and b of Figure 1 show two TEM BF images for lamellar single crystals of PEO-*b*-PS(11.0K−4.6K) grown in the mixed solvent at $T_x = 25$ °C and PLLA-*b*-PS-(19.9K−9.2K) grown in amyl acetate at $T_x = 72$ °C, respectively. Two SAED patterns have also been inserted in these two figures. In Figure 1a, the PEO-*b*-PS single crystal exhibits a square-shape bound by four (120) planes. A lozenge-shaped single crystal is observed for the PLLA-*b*-PS grown in amyl acetate, as shown in Figure 1b. The single crystal is bound by four (110) planes. These crystal habits in Figure 1a,b are identical with those observed in PEO and PLLA homopolymer single crystals.[15,16,55,59−61] Moreover, these two SAED patterns are recognized to be the [001] zone patterns of the monoclinic lattice of PEO[15,16,59,60] and the orthorhombic lattice (α-form) of PLLA[55,61] homopolymer single crystals, indicating that the chain directions in both "sandwiched" crystals are parallel to their lamellar surface normal. All other copolymers listed in Tables 1 and 2 can also grow single crystals, as shown in Figure 1a,b.

We first used PEO and PLLA homopolymers to grow single crystals at different isothermal T_x values in amyl acetate dilute solutions. Their lamellar thicknesses were measured using AFM.

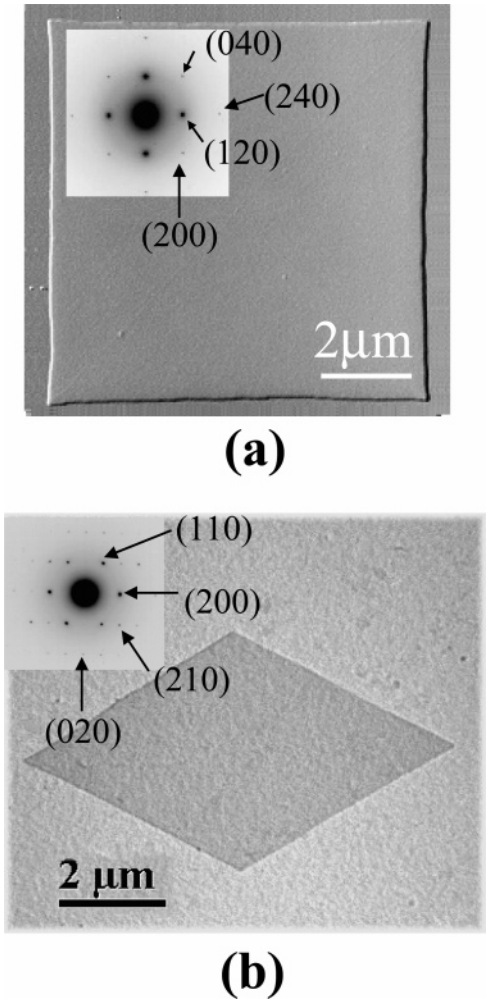

Figure 1. TEM BF images of lamellar single crystals of PEO-*b*-PS-(11.0K−4.6K) (sample 3 in Table 1) in chlorobenzene/octane mixed solution at $T_x = 25$ °C (a) and of PLLA-*b*-PS(19.9K−9.2K) (sample 15 in Table 2) in amyl acetate solution at $T_x = 72$ °C (b).

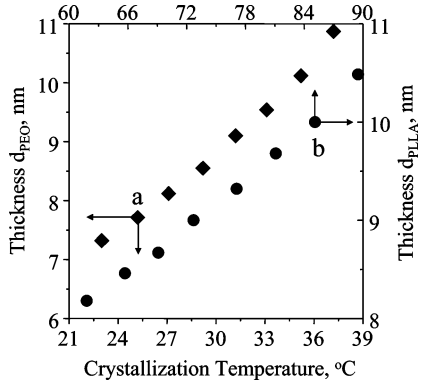

Figure 2. Relationships between the lamellar crystal thickness and T_x values for both the homo-PEO (a) and homo-PLLA (b) fractions.

Figure 2 shows two sets of lamellar crystal thickness (d_{CRYST}) data with changing T_x values for both the PEO and PLLA homopolymers. Despite the different dependencies of d_{CRYST} on T_x for these two homopolymers, both sets of data exhibit a general trend that the d_{CRYST} values increase with increasing T_x. These data fit well with the known behaviors of polymer single crystals grown in dilute solutions reported previously.[53]

The $d_{OVERALL}$ values of the "sandwiched" lamellar single crystals of the PEO-*b*-PS and PLLA-*b*-PS diblock polymers were measured using AFM, and the d_{PEO} and d_{PLLA} values can be calculated on the basis of eq 1a. The question is: can we provide experimental evidence to confirm that the calculated d_{PEO} and d_{PLLA} values are correct? An experiment was designed to answer this question. We used the PEO-*b*-PS or PLLA-*b*-PS single crystals as seeds to further grow PEO or PLLA homopolymer single crystals on the seeds. Note that the homopolymers can only nucleate on the facetted growth fronts of the middle, single-crystal layer of the diblock copolymer seeds with the identical chain orientation and thickness. Namely, for the PEO homopolymer, it grows on the (120) planes of the middle layer of the "sandwiched" single-crystal seeds, while the PLLA homopolymer grows on the (110) planes of the copolymer seeds.

Figure 3 represents an experimental observation of a composite single crystal using PLLA-*b*-PS(56.8K−9.2K) and the PLLA homopolymer. In Figure 3a, a lozenge-shaped lamellar single crystal with two different thicknesses is observed using the height image of AFM. The center thicker part is the block copolymer "sandwiched" single-crystal grown in amyl acetate at $T_x = 72$ °C. The outside facetted, thinner single crystal is the further growth of the PLLA homopolymer at the same T_x. Figure 3b illustrates a height profile of these two parts of the single crystal measured via AFM, and at the conjunction between the PLLA-*b*-PS and PLLA homopolymer single crystals, the thickness of the PLLA homopolymer crystal is 9.0 nm (Figure 3c is the enlarged height profile near the conjunction). Furthermore, with increasing the crystallization time, as shown in Figure 3b,c, the height of the PLLA homopolymer single crystal gradually increases, and finally, it reaches 9.5 nm. This is due to the fact that the lowest nucleation barrier for the PLLA homopolymer to overcome at $T_x = 72$ °C is associated with a greater value of the lamellar thickness compared with that for the PLLA-*b*-PS copolymer. However, at the conjunction, the PLLA homopolymer has to be confined to a thickness provided by the (110) growth front of the PLLA-*b*-PS copolymer.

Using AFM, we can measure $d_{OVERALL}$ thicknesses of the copolymer single crystals. The difference between the $d_{OVERALL}$ and the conjunction which connects the copolymer with the homopolymer single crystals is d_{PS}. The PEO or PLLA homopolymer lamellar crystal thickness at the conjunctions can be obtained since it is equal to $d_{OVERALL} - 2d_{PS}$. These homopolymer lamellar thicknesses at the conjunctions thus serve as experimentally measured d_{PEO} or d_{PLLA} values for the diblock copolymer crystal layer. The homo-PLLA part of the composite single crystals may completely slip down on to the glass substrates, as shown in Figure 3. In this case, the thicknesses measured at the conjunctions of the copolymer seeds is a direct measure of the d_{PLLA}. The measured experimental value is 9.0 nm, and the calculated d_{PLLA}, based on eq 1a in this case, is also 9.0 nm, showing good agreement between observation and calculation. To obtain the complete slippage, which provides the most consistent result, gentle vertical vibrations of the samples were generated by a piezoelectric element.

Figure 4 shows a sequentially crystallized composite single crystal of PEO-*b*-PS(20.3K−6.8K) and PEO homopolymer at $T_x = 35.0$ °C in amyl acetate. The square-shaped single crystal is observed in the AFM height image. The center, thicker part is the block copolymer single crystal, and the outside, thinner part of the composite single crystal is attributed to the PEO homopolymer (Figure 4a). Figure 4b represents a height profile of the composite single crystal and the thickness of the PEO homopolymer single crystal at the conjunction (Figure 4c is the enlarged height profile near the conjunction). The d_{PEO} value

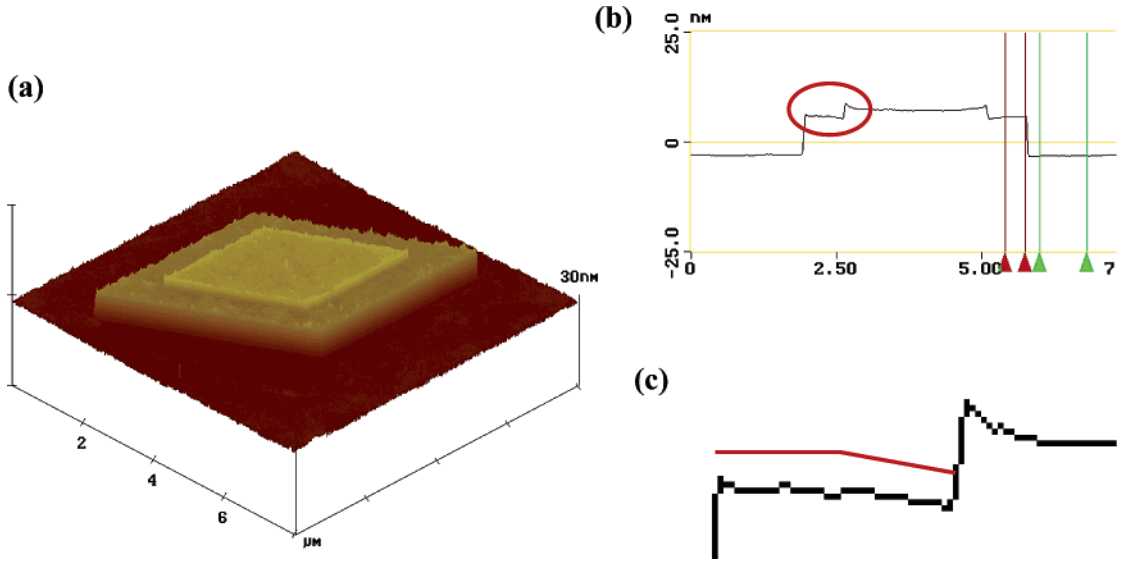

Figure 3. AFM micrographs of a homo-PLLA single-crystal grown from a PLLA-*b*-PS(56.8K−9.2K) (sample 13 in Table 2) seed: (a) the three-dimensional height view; (b) a two-dimensional height view; (c) an enlarged height view at the connection point between the PLLA-*b*-PS seed and homo-PLLA single crystal. The thickness of the homo-PLLA single crystal at the connection point is 9.0 nm.

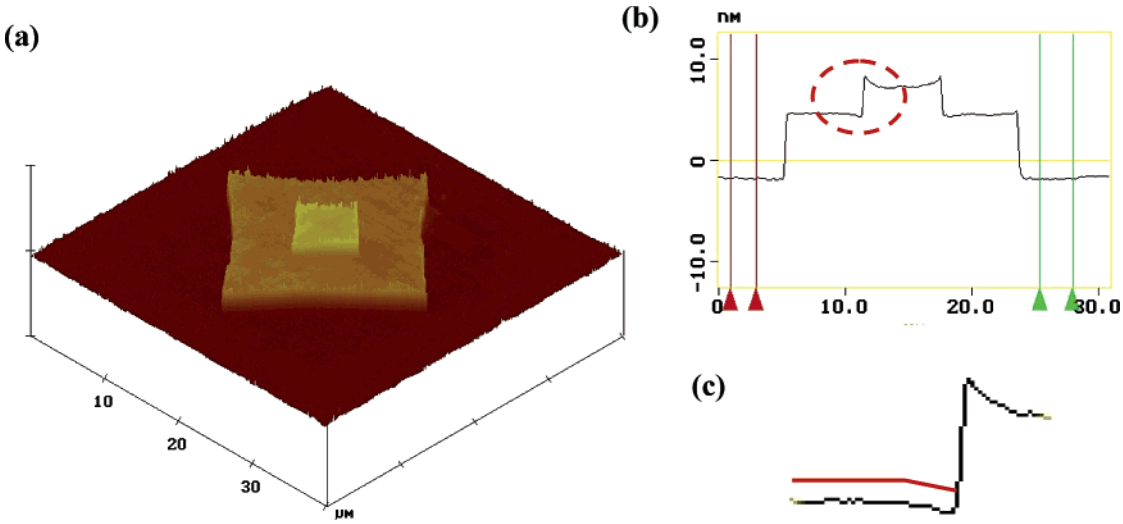

Figure 4. AFM micrographs of a homo-PLLA single-crystal grown from a PEO-*b*-PS(20.3K−6.8K) (sample 7 in Table 1) seed: (a) the three-dimensional height view; (b) a two-dimensional height view; (c) an enlarged height view at the connection point between the PEO-*b*-PS seed and homo-PEO single crystal. The thickness of the homo-PEO single crystal at the connection point is 8.9 nm.

is 8.9 nm, which can be compared with the calculated d_{PEO} value of 8.9 nm based on eq 1a. This indicates, again, that our calculation based on eq 1a is reliable. For all the copolymers, their calculated d_{PEO} and d_{PLLA} values were identical to the experimentally observed thicknesses in multiple repeated measurements without exceptions.

Figure 5 shows relationships between the experimental d_{PEO} values and T_x for four different PEO-*b*-PS diblock copolymers with different MW's crystallized in two different solutions (the mixed solvent and amyl acetate) as examples. PEO-*b*-PS(11.0K−4.6K) was grown in chlorobenzene/octane, and the other three samples [PEO-*b*-PS(17.0K−3.0K, 40.1K−7.7K, and 20.3K−6.8K)] were grown in amyl acetate. Three types of behavior for the d_{PEO} changes with T_x can be observed. First, PEO-*b*-PS(17.0K−3.0K) in amyl acetate behaves similar to the PEO homopolymer. Second, PEO-*b*-PS(11.0K−4.6K) in the mixed solvent and PEO-*b*-PS(40.1K−7.7K) in amyl acetate exhibit increases of their d_{PEO} values with T_x in the low-T_x region until a T_x* is reached. For PEO-*b*-PS(11.0K−4.6K), the T_x* = 27.2 °C, while for PEO-*b*-PS(40.1K−7.7K), the T_x* = 28.3 °C. Below the T_x*, the d_{PEO} changes are similar to that of the PEO

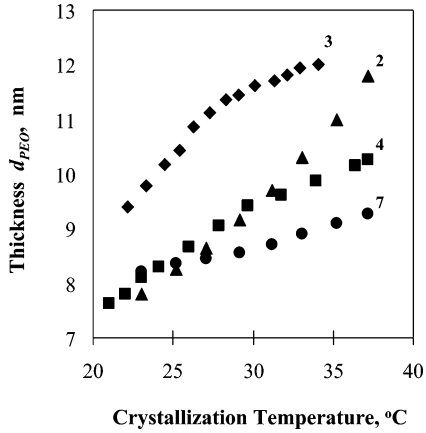

Figure 5. Relationships between the d_{PEO} and T_x for four PEO-*b*-PS diblock copolymer samples crystallized at different T_x values. From top to bottom, they are PEO-*b*-PS(11.0K−4.6K) (sample 3 in Table 1) in chlorobenzene/octane mixed solvent, PEO-*b*-PS(17.0K−3.0K) (sample 2) in amyl acetate, PEO-*b*-PS(40.1K−7.7K) (sample 4) in amyl acetate, and PEO-*b*-PS(20.3K−6.8K) (sample 7) in amyl acetate.

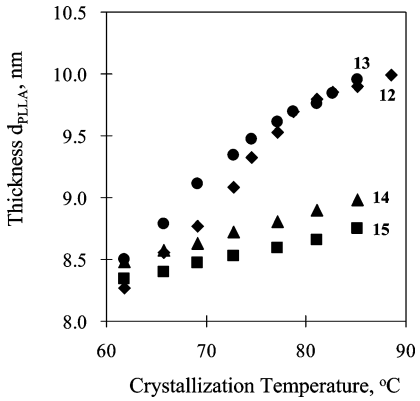

Figure 6. Relationships between d_{PLLA} and T_x for four PLLA-*b*-PS diblock copolymers crystallized at different T_x values in amyl acetate. From top to bottom PLLA-*b*-PS(56.8K−9.2K) (sample 13 in Table 2), PLLA-*b*-PS(27.3K−6.0K) (sample 12), PLLA-*b*-PS(31.8K−9.2K) (sample 14), and PLLA-*b*-PS(19.9K−9.2K) (sample 15).

homopolymer as shown in Figure 2a and that of PEO-*b*-PS-(17.0K−3.0K) in Figure 5. Above the T_x*, both of the d_{PEO}'s suddenly reduce their dependence on T_x. Third, the d_{PEO} values of PEO-*b*-PS(20.3K−6.8K) only slightly increases with T_x in the whole T_x region studied. No sudden change of the d_{PEO} values is found. The slope of this d_{PEO} increase with T_x for PEO-*b*-PS(20.3K−6.8K) is similar to those of the other two samples above their T_x* values. For all the samples shown in Table 1, the d_{PEO} changes with T_x have been measured for the single-crystal grown in amyl acetate and/or the mixed solvent. Their behaviors always belong to one of these three types described.

Four relationships between the d_{PLLA} values and T_x are shown in Figure 6 for PLLA-*b*-PS copolymers with different MW's: PLLA-*b*-PS(56.8K−9.2K, 31.8K−9.2K, 27.3K−6.0K, and 19.9K−9.2K). All of these diblock copolymer single crystals were grown in amyl acetate. It is evident that PLLA-*b*-PS-(56.8K−9.2K) and PLLA-*b*-PS(27.3K−6.0K) in Figure 6 exhibit the sudden reduction of the d_{PLLA} dependence at T_x* = 78 and 72 °C, respectively. They belong to the second type of behavior in the PEO-*b*-PS samples shown in Figure 5. The other two samples PLLA-*b*-PS(31.8K−9.2K and 19.9K−9.2K) only show slight increases of the d_{PLLA} values with T_x. They are identified to be the third type of behavior in Figure 5, and their slopes are, again, similar to those of PLLA-*b*-PS(56.8K−9.2K) and PLLA-*b*-PS(27.3K−6.0K) above their T_x* values.

By knowing the d_{CRYST}, ρ_{CRYST}, and M_n^{CRYST}, the σ values can be calculated on the basis of eq 2. Since the R_g values of the PS homopolymers with different MWs in both solvents are known (determined via light scattering),[62] the $\tilde{\sigma}$ can also be obtained. For the copolymers listed in Tables 1 and 2, we can generate a wide range of $\tilde{\sigma}$ from close to 0 up to 24. This $\tilde{\sigma}$ range should be broad enough to cover from the "noninteraction" regime where the tethered chains are independent from each other to the "highly stretched brush" regime where the tethered chains exhibit their stretched conformations along the surface normal direction.

Relationships between $1/d_{CRYST}$ Values and T_x for Homopolymer and Copolymer Single Crystals. We further examine quantitative relationships between d_{CRYST} and T_x for the PEO and PLLA homopolymers. In principle, the d_{CRYST} of homopolymer single crystals should be proportional to the reciprocal undercooling, $1/\Delta T$. Namely, the d_{CRYST} follows a linear relationship with $1/\Delta T$:[63−65]

$$d_{CRYST} = \frac{2\gamma_e T_d}{\Delta h_d \Delta T} = \frac{2\gamma_e T_d}{\Delta h_d (T_d - T_x)} \quad (3)$$

where T_d is the equilibrium dissolution temperature, γ_e is the folded surface free energy, and Δh_d is the equilibrium heat of dissolution. When we plot relationships between the reciprocal thicknesses vs isothermal T_x values for these two homopolymers, two linear relationships can be observed (see below in Figures 7 and 8). This is a simple rearrangement of eq 3:

$$\frac{1}{d_{CRYST}} = \frac{\Delta h_d \Delta T}{2\gamma_e T_d} = \frac{\Delta h_d}{2\gamma_e} - \frac{\Delta h_d}{2\gamma_e T_d} T_x \quad (4)$$

The slope of this relationship ($1/d_{CRYST}$ vs T_x) is equal to $-\Delta h_d/(2\gamma_e T_d)$, indicating that the reciprocal thickness is proportional to the reciprocal γ_e. These two sets of data will be used as the references to compare with the d_{PEO} and d_{PLLA} values of the single crystals in our two series of diblock copolymers grown in dilute solutions.

Figures 7 and 8 represent relationships between $1/d_{CRYST}$ ($1/d_{PEO}$ or $1/d_{PLLA}$) and T_x for the complete data set of the homopolymers and the copolymers we have measured. Figure 7 includes a homo-PEO and nine PEO-*b*-PS copolymers crystallized in amyl acetate or the mixed solvent. Both the homo-PEO and a PEO-*b*-PS(17K−3.0K) with the low M_n^{PS} exhibit single linear relationships between $1/d_{PEO}$ and T_x throughout the T_x range. Their slopes are almost identical, indicating that the short PS chains do not significantly affect the γ_e value compared with that of the PEO homopolymer single crystals. By increasing the ratio between M_n^{PS} and M_n^{PEO}, the second type of behavior possessing two slopes can be found in the $1/d_{PEO}$ vs T_x plot for PEO-*b*-PS(11.0K−4.6K) in the mixed solvent and for PEO-*b*-PS(40.1K−7.7K) and PEO-*b*-PS(23.0K−6.0K) in amyl acetate. The slope changes in these samples occur at $\tilde{\sigma}^* = 3.7$, as reported previously.[18] When $\tilde{\sigma} < 3.7$, the slopes of these two samples are close to those of the homo-PEO and PEO-*b*-PS(17K−3.0K). These results imply that below $\tilde{\sigma} = 3.7$ the PS blocks do not influence the γ_e value. When $\tilde{\sigma} > 3.7$, the PS blocks start to influence the d_{PEO} via an effect on the γ_e value as evidenced by the appearance of the second slope in these two copolymers. For the rest of the copolymers, which have increasingly large M_n^{PS}/M_n^{PEO} (all are in amyl acetate), the third type of behavior, namely, only a single linear relationship can be observed for each sample. Quantitative study shows that the absolute values of the slopes in these copolymers decrease with increasing M_n^{PS}/M_n^{PEO}. These observations indicate that the single crystals of these copolymers must possess $\tilde{\sigma} > 3.7$ in the T_x region studied; therefore, the $\tilde{\sigma}^* = 3.7$ has to appear at lower values of T_x. Furthermore, as the M_n^{PS}/M_n^{PEO} value increases, the d_{PEO} value at $\tilde{\sigma}^* = 3.7$ (d_{PEO}*) should also decrease. This can be understood by the fact that at $\tilde{\sigma}^* = 3.7$ the d_{PEO}* is proportional to $M_n^{PEO}/(R_g^{PS})^2$. Note that the $(R_g^{PS})^2$ is proportional to $(M_n^{PS})^{6/5}$. Namely, with increasing the M_n^{PS}/M_n^{PEO}, the PS block requires a larger covering area and thus a bigger number of folds of the PEO crystal; i.e., a smaller d_{PEO}* is needed to keep a constant entropic repulsion generated by the tethered PS chains at $\tilde{\sigma}^*$.

Similar observations are found in a series of PLLA-*b*-PS single crystals grown in amyl acetate, as shown in Figure 8. The homo-PLLA possesses a single linear relationship in the plot between $1/d_{PLLA}$ and T_x, while PLLA-*b*-PS(56.8K−9.2K) and PLLA-*b*-PS(27.3K−6.0K) have two slopes that can be observed in the T_x region studied. Again, the slope changes occur

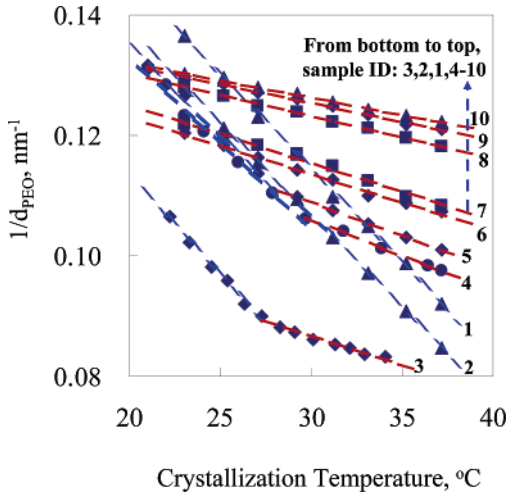

Figure 7. Relationships between $1/d_{PEO}$ and T_x for 10 PEO-*b*-PS diblock copolymer (and PEO homopolymer) samples crystallized at different T_x values in both chlorobenzene/octane (for sample 3 in Table 1 only) and amyl acetate (for samples 2−10). From bottom to the top samples 1−10 are (3) PEO-*b*-PS (11.0K−4.6K), (2) PEO-*b*-PS (17.0K−3.0K), (1) PEO homopolymer, (4) PEO-*b*-PS (40.1K−7.7K), (5) PEO-*b*-PS (23.0K−5.0K), (6) PEO-*b*-PS (16.7K−5.0K), (7) PEO-*b*-PS (20.3K−6.8K), (8) PEO-*b*-PS (9.4K−6.7K), (9) PEO-*b*-PS (8.7K−9.2K), and (10) PEO-*b*-PS (17.0K−11.0K).

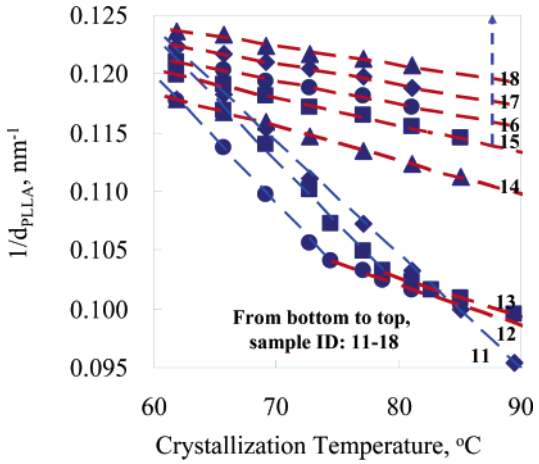

Figure 8. Relationships between $1/d_{PLLA}$ and T_x for eight PLLA-*b*-PS diblock copolymer (and PLLA homopolymer) samples crystallized at different T_x values in amyl acetate. From bottom to top samples 11−18 are (11) PLLA homopolymer, (12) PLLA-*b*-PS (27.3K−6.0K), (13) PLLA-*b*-PS (56.8K−9.2K), (14) PLLA-*b*-PS (31.8K−9.2K), (15) PLLA-*b*-PS (19.9K−9.2K), (16) PLLA-*b*-PS (15.0K−9.2K), (17) PLLA-*b*-PS (11.0K−9.2K), and (18) PLLA-*b*-PS (18.0K−19.3K).

at $\tilde{\sigma}^* = 3.7$. The slopes of these samples, in the region where $\tilde{\sigma} < 3.7$, are similar to that of the PLLA homopolymer. Only one slope can be observed with a further increase in the M_n^{PS}/M_n^{PLLA}, as is the cases for the rest of the copolymers. Again, the absolute value of the slope decreases with an increase in the M_n^{PS}/M_n^{PLLA}.

It can be concluded that our observations of the d_{CRYST} value changes with T_x in single crystals of these two sets of copolymers can reflect the changes of interactions of the PS tethered chains. In Figures 7 and 8, the slope changes at the T_x^* for each of those five copolymer samples occur at $\tilde{\sigma}^* = 3.7$, disregarding the different types of crystalline blocks, different MW's, and different solvents used. A qualitative explanation is that at $\tilde{\sigma}^* = 3.7$ the tethered PS chains start to interact with each other and generate repulsion. The interaction hampers the increase of the d_{PEO} or d_{PLLA} during single-crystal growth of the PEO or PLLA blocks. A much slower increase of these d_{PEO} or d_{PLLA} values can thus be observed (decrease in the slope). The physical meaning of this $\tilde{\sigma}^*$ value is when an area which is covered by a single PS tethered chain (πR_g^2) statistically accommodates 3.7 chains, the PS chains start to feel that they are overcrowded by their neighbors. Therefore, this should be the onset of tethered chain overcrowding.[18] When $\tilde{\sigma} < 3.7$, the PS chains are in the noninteraction regime.

Other PEO-*b*-PS and PLLA-*b*-PS copolymers having larger ratios of the M_n^{PS}/M_n^{PEO} and the M_n^{PS}/M_n^{PLLA} in Figures 7 and 8 possess single slopes in the T_x range. Our calculations indicate that the $\tilde{\sigma}$ values for these copolymer single crystals possess values greater than 3.7 (up to 24); therefore, the number of folds for these crystalline blocks does not generate enough covering area for the tethered PS chains to be free of interaction. The repulsion caused by the interactions of the tethered PS chains is, as a result, remarkably high and prevents a normal increase of the d_{PEO} and d_{PLLA} in these $T_x > T_x^*$ regions compared to the observations in the homopolymer single crystals, PEO-*b*-PS (17.0K−3.0K), and those five copolymers below their T_x^* values. It should be noted that a more precise representation of these interactions with T_x, in theory, should obey an exponential law relation. The fact that observed linear relationships in Figures 7 and 8 with constant slopes when $\tilde{\sigma} > 3.7$ indicates that the γ_e values exhibit little changes with T_x in the T_x region studied. This is certainly a first approximation to illustrate that within the T_x region the interaction generated by the PS chains are close to constant. Therefore, eq 4 can also be used to calculate the γ_e values based on the slopes of these linear relationships because the other parameters (Δh_d and T_d) are kept to be invariant, and only the γ_e values possess a sudden increase at $\tilde{\sigma}^* = 3.7$.

Reduced Surface Free Energy. How can we quantitatively understand this interaction among the tethered PS chains? Let us first consider the components in the surface free energy term, γ_e. For a single crystal of a diblock copolymer, the γ_e consists of three contributions: $\gamma_e = \gamma_{CRYST/PS} + \gamma_{PS} + \gamma_{PS/SOLVENT}$, where $\gamma_{CRYST/PS}$ and $\gamma_{PS/SOLVENT}$ are the interfacial energies at the crystal/PS and PS/solvent interfaces, and γ_{PS} is the contribution generated by the interaction among the tethered PS chains. In our experiments, the PEO or PLLA crystal surfaces do not favor interaction with the PS blocks; therefore, there are always more solvent/crystal contacts than PS/crystal contacts, and it is reasonable to assume that $\gamma_{CRYST/PS}$ is equal to the surface free energy of the homopolymer single crystal γ_{CRYST}. For a good or θ solvent, the contribution $\gamma_{PS/SOLVENT}$ can also be ignored when compared with γ_{CRYST}. The total γ_e is thus close to the γ_{PEO} or γ_{PLLA} in the noninteraction region. This is supported by the experimental observation that the slopes of some diblock copolymers are the same as the homopolymer in the noninteraction region. On the basis of the above assumptions, the γ_e can be simplified to $\gamma_e = \gamma_{CRYST} + \gamma_{PS}$. For a given copolymer sample which exhibits two linear relationships, the γ_e can be calculated in these two T_x regions (below and above T_x^*).

We now need a quantity of relative surface free energy utilizing the homopolymers as references. This can be approximated by a ratio between the two slopes of the copolymers and the homopolymers. For example, for PEO-*b*-PS copolymers we use the ratio of γ_e/γ_{PEO} and for PLLA-*b*-PS copolymers, γ_e/γ_{PLLA}. The contribution from the tethered PS chains can thus be presented by an average reduced surface free energy: $\Gamma^{PS} = \gamma_e/\gamma_{PEO} - 1$ or $\gamma_e/\gamma_{PLLA} - 1$ for both series of copolymers. This value is dimensionless, and for PEO and PLLA homopolymers, $\Gamma^{PS} = 0$. For the PEO-*b*-PS and PLLA-*b*-PS copolymers in the "noninteraction" regime, Γ^{PS} is also 0. This has been

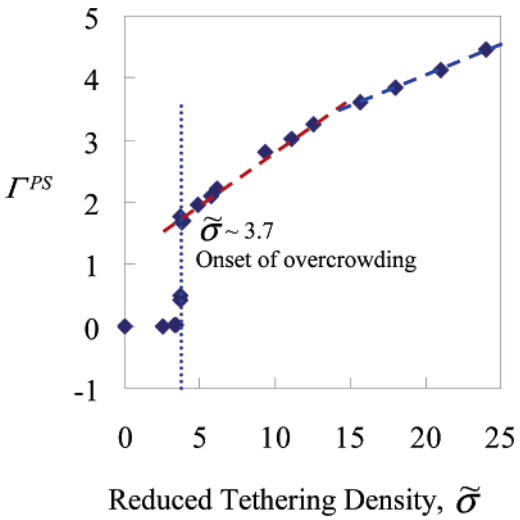

Figure 9. Relationship between the Γ^{PS} and $\tilde{\sigma}$ values for both series of PEO-*b*-PS and PLLA-*b*-PS diblock copolymers crystallized in dilute solutions.

experimentally confirmed in Figures 7 and 8 since, for the five copolymers below T_x* values, the slopes of these copolymers are almost identical to those of the homopolymer single crystals. For those diblock copolymers with the PS tethered chains which are interacting with each other, $\Gamma^{PS} > 0$, and the Γ^{PS} value increases as the interactions among the tethered PS chains increases. For example, as calculated from the data of PEO-*b*-PS(40.1K−7.7K) grown in amyl acetate (Figure 7), the $\Gamma^{PS} = 0$ when $T_x < T_x$*, and the $\Gamma^{PS} = 1.8$ when $T_x > T_x$*.

It should also be noted that at different T_x values for the single-crystal growth of a specific diblock copolymer when $\tilde{\sigma} > 3.7$, the $\tilde{\sigma}$ value should change. However, in all of these diblock copolymers, their $\tilde{\sigma}$ changes in the entire T_x region is smaller than one. When PEO-*b*-PS(20.3K−6.8K) was crystallized between $T_x = 23.0$ and 37.2 °C, e.g., the $\tilde{\sigma}$ value changes from 5.8 to 6.4. Since experimental observations of the relationships between the $1/d_{CRYST}$ and T_x are linear and the $\tilde{\sigma}$ value change for each diblock copolymer is relatively narrow within the T_x range studied, an average γ_e value and, thus, an average Γ^{PS} value at an average $\tilde{\sigma}$ [for PEO-*b*-PS(20.3K−6.8K), e.g., the average $\tilde{\sigma} = 6.1$] for each of the diblock copolymers are used to represent the interaction of tethered PS chains on the crystal surface.

Since the γ_{PEO} is different from the γ_{PLLA} based on the experimental data shown in Figures 7 and 8, we also need to normalize these two sets of data for PEO-*b*-PS and PLLA-*b*-PS copolymers. Furthermore, we assume that the additional surface free energy caused by the repulsion of the PS tethered chains is independent of the type of crystal substrates (PEO or PLLA) for both series of copolymers. The normalization factor can thus be estimated to be about 0.8 for the Γ^{PS} values obtained in the series of PLLA-*b*-PS diblock copolymers compared with those obtained in the series of PEO-*b*-PS copolymers.

Figure 9 shows a plot between the normalized Γ^{PS} vs $\tilde{\sigma}$ values obtained from the single crystals grown in amyl acetate for both series of PEO-*b*-PS and PLLA-*b*-PS copolymers. When the $\tilde{\sigma}$ increases from 0 to 3.7, the Γ^{PS} values keep to zero, indicating that the PS tethered chains are in the noninteraction regime. Note that the $\tilde{\sigma} = 1$ represents the case where the neighboring PS tethered chains start to touch each other. When $1 < \tilde{\sigma} < 3.7$, more than one PS tethered chain is in the covered area of πR_g^2, but no repulsion is generated. At $\tilde{\sigma}^* = 3.7$, the Γ^{PS} values jump to 1.8, revealing that the tethered PS chains at this $\tilde{\sigma}$ suddenly "feel" overcrowded by their neighbors, and the repulsion of the PS chains provides a significant contribution to the Γ^{PS}. This behavior is similar to the hard-sphere-like interaction model.[66] After this sudden transition, the Γ^{PS} continuously increases with $\tilde{\sigma}$. The Γ^{PS} continuously increases with $\tilde{\sigma}$ until it reaches 4.5 at $\tilde{\sigma} = 24$. This Γ^{PS} increase can be described by two linear relationships with different slopes. The first linear relationship ends at $\tilde{\sigma} = 14.3$, and then the slope suddenly decreases when $\tilde{\sigma} > 14.3$. This may reveal that further increases of the $\tilde{\sigma}$ leads to the layer thickness increase of the PS tethered chains due to the extension of chain conformation deviated from the coils. The question is: how do we judge whether this slope change at $\tilde{\sigma} = 14.3$ corresponds to the onset of the highly stretched brush regime based on our experimental observations?

Where Does the Highly Stretched Brush Regime Start? In the highly stretched brush regime of tethered polymer chains in a good solvent (such as PS chains in amyl acetate) without the adsorption interaction between tethered chains and the substrate, the scaling law suggests that overall free energy cost per tethered chain (f) with a length of N is attributed to a balance between the entropic effect of the tethered chain, which has to be deviated from the unperturbated coil chain conformation, and the favorable interaction of the tethered chain with the good solvent. The free energy cost can be expressed as follows:[38−42]

$$f \sim kT\left(\frac{3l^2}{2Na^2} + \frac{\nu N^2 a^3 \sigma}{l}\right) \quad (5)$$

where the l is the thickness of the tethered chain layer in solution, υ is the excluded volume parameter, and a is the segmental size of the tethered chain. The equilibrium thickness, l, can be obtained by a minimization of the f with respect to l in eq 5:

$$l_{eq} = 3^{-1/3} N \nu^{1/3} a^{5/3} \sigma^{1/3} \quad \text{and} \quad f_{eq} \sim \frac{3^{4/3}}{2} kTN a^{4/3} \nu^{2/3} \sigma^{2/3} \quad (6)$$

Since the f_{eq} is the free energy cost for a single tethered chain, whose covering area is $1/\sigma$, at equilibrium, the free energy per unit area resulting from the tethered chains can be expressed as

$$\gamma_{PS} = f_{eq}\sigma \sim kT(Na^2\nu^{2/3}\sigma)a^{-2/3}\sigma^{2/3} \sim kT\tilde{\sigma}a^{-2/3}\sigma^{2/3} \quad (7)$$

Note that this scaling relation can only be applicable in the highly stretched brush regime. The left side of eq 7 can be obtained in our experimental data Γ^{PS}, since $\gamma_{PS} = \Gamma^{PS}\gamma_{PEO}$ (or γ_{PLLA}). In the right side of this equation, the parameters k and a are constants, the $T = T_x$, and σ and $\tilde{\sigma}$ can be calculated. Using a new variable, $x = T\tilde{\sigma}\sigma^{2/3}$, eq 7 can be rearranged to be a linear relationship between Γ^{PS} and x. By definition, in the highly stretched brush regime of the experimental tethered chains, the plot of the Γ^{PS} and x should fit into a linear relationship with a nonzero slope and a zero intercept.

Figure 10 shows the linear relationship between the Γ^{PS} and x (the dashed line) and the experimental data for both series of PEO-*b*-PS and PLLA-*b*-PS copolymers crystallized in amyl acetate. In the regime where the x values are low, the Γ^{PS} keeps near 0, corresponding to the noninteraction regime; as the x values increase, the Γ^{PS} value increases almost vertically at $\tilde{\sigma}^* = 3.7$ (equivalent to $x = 220$). This is the onset of the tethered chain overcrowding, which can be described as a hard-sphere-like interaction. It is evident in Figure 10 that when the $\tilde{\sigma}$ value is below 3.7, the scaling laws' prediction overestimates the free

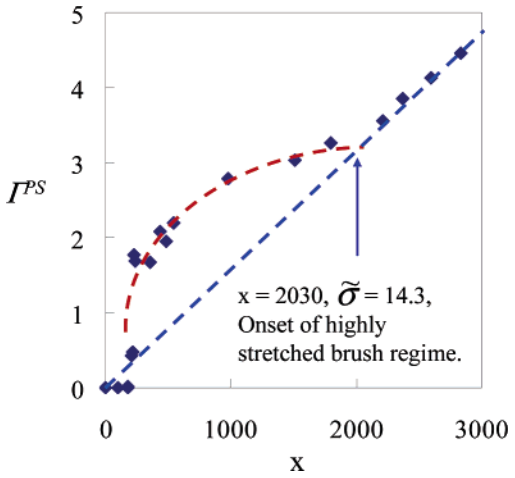

Figure 10. Comparison of experimental data with the prediction of the scaling law. The linear relationship between the Γ^{PS} and x ($x = T\tilde{\sigma}\sigma^{2/3}$) values is predicted by the scaling laws (dashed line), and the points are based on experimental observations.

energy of the PS chains' interactions. When the $\tilde{\sigma} > 14.3$, the experimental data fit well with the prediction of the scaling laws. This suggests that the highly stretched brush regime for the tethered PS chains starts at $\tilde{\sigma}^{**} = 14.3$. Therefore, between $\tilde{\sigma}^{*} = 3.7$ and $\tilde{\sigma}^{**} = 14.3$, a crossover regime can be identified. In this regime, the scaling laws' prediction underestimates the free energy of the PS chains' interactions. It is worth while to note that entering the highly stretched brush regime for the tethered PS chains exhibits a continuous transition.

Conclusion

In summary, we have designed an experiment using crystalline−amorphous diblock copolymers, such as PEO-*b*-PS and PLLA-*b*-PS copolymers, to detect the interaction changes of the tethered PS chains on the PEO or PLLA single crystal basal surface. This method can generate a broad range of uniformly controlled $\tilde{\sigma}$. Using the crystal layer thickness changes in the copolymer single crystals (d_{PEO} and d_{PLLA}) as probes, three regimes can be identified on the basis of the different interaction behaviors of the tethered PS chains: the noninteraction, the crossover, and the highly stretched regimes. It has been found that the tethered PS chains are in the noninteraction regime until $\tilde{\sigma}$ reaches 3.7 ($\tilde{\sigma}^{*}$). This is the onset of the tethered PS chain overcrowding. It is the discontinuous transition from the noninteracting to the crossover regime when the relationship between reduced surface free energy, Γ^{PS}, and $\tilde{\sigma}$ is plotted. Experimental observations also provide evidence for the onset of the highly stretched brush regimes of the tethered PS chains, which takes place at $\tilde{\sigma} = 14.3$ ($\tilde{\sigma}^{**}$). The Γ^{PS} experimental data fit the prediction of scaling laws of tethered PS chains after $\tilde{\sigma}^{**} \geq 14.3$, proving the transition to the highly stretched brush regime. This onset, unlike the overcrowding transition, is a continuous transition based on the Γ^{PS} and $\tilde{\sigma}$ relation.

Acknowledgment. This work was supported by NSF (DMR-0516602). Light scattering experiments were kindly carried out by collaborators with Prof. Chi Wu's laboratory at Chinese University of Hong Kong. Extensive and helpful discussions with Dr. Freddy Khoury and Dr. Edward DeMarzio are greatly appreciated.

References and Notes

(1) Cohen, R. E.; Cheng, P. L.; Douzinas, K. C.; Kofinas, P.; Berney, C. V. *Macromolecules* **1990**, *23*, 324.
(2) Rangarajan, P.; Register, R. A.; Fetters, L. J. *Macromolecules* **1993**, *26*, 4640.
(3) Khandpur, A. K.; Macosko, C. W.; Bates, F. S. *J. Polym. Sci., Polym. Phys. Ed.* **1995**, *33*, 247.
(4) Yang, Y. W.; Tanodekaew, S.; Mai, S.-M.; Booth, C.; Ryan, A. J.; Bras, W.; Viras, K. *Macromolecules* **1995**, *28*, 6029.
(5) Hamley, I. W.; Fairclough, J. P. A.; Ryan, A. J.; Bates, F. S.; Towns-Andrews, E. *Polymer* **1996**, *37*, 4425.
(6) Hamley, I. W.; Fairclough, J. P. A.; Terrill, N. J.; Ryan, A. J.; Lipic, P. M.; Bates, F. S.; Towns-Andrews, E. *Macromolecules* **1996**, *29*, 8835.
(7) Quiram, D. J.; Register, R. A.; Marchand, G. R.; Ryan, A. J. *Macromolecules* **1997**, *30*, 8338.
(8) Zhu, L.; Chen, Y.; Zhang, A.; Calhoun, B. H.; Chun, M.; Quirk, R. P.; Cheng, S. Z. D.; Hsiao, B. S.; Yeh, F.; Hashimoto, T. *Phys. Rev. B* **1999**, *60*, 10022.
(9) Zhu, L.; Cheng, S. Z. D.; Calhoun, B. H.; Ge, Q.; Quirk, R. P.; Thomas, E. L.; Hsiao, B. S.; Yeh, F.; Lotz, B. *J. Am. Chem. Soc.* **2000**, *122*, 5957.
(10) Loo, Y. L.; Register, R. A.; Ryan, A. J.; Dee, G. T. *Macromolecules* **2001**, *34*, 8968.
(11) Huang, P.; Zhu, L.; Cheng, S. Z. D.; Ge, Q.; Quirk, R. P.; Thomas, E. L.; Lotz, B.; Hsiao, B. S.; Liu, L.; Yeh, F. *Macromolecules* **2001**, *34*, 6649.
(12) Loo, Y. L.; Register, R. A.; Ryan, A. J. *Macromolecules* **2002**, *35*, 2365.
(13) Zhu, L.; Huang, P.; Chen, W. Y.; Ge, Q.; Quirk, R. P.; Cheng, S. Z. D.; Thomas, E. L.; Lotz, B.; Hsiao, B. S.; Yeh, F.; Liu, L. *Macromolecules* **2002**, *35*, 3553.
(14) Huang, P.; Zhu, L.; Guo, Y.; Ge, Q.; Jing, A. J.; Chen, W. Y.; Quirk, R. P.; Cheng, S. Z. D.; Thomas, E. L.; Lotz, B.; Hsiao, B. S.; Avila-Orta, C. A.; Sics, I. *Macromolecules* **2004**, *37*, 3689.
(15) Lotz, B.; Kovacs, A. J. *Kolloid Z. Z. Polym.* **1966**, *209(2)*, 97.
(16) Lotz, B.; Kovacs, A. J.; Bassett, G. A.; Keller, A. *Kolloid Z. Z. Polym.* **1966**, *209*, 115.
(17) Chen, W. Y.; Li, C. Y.; Zheng, J. X.; Huang, P.; Zhu, L.; Ge, Q.; Quirk, R. P.; Lotz, B.; Deng, L.; Wu, C.; Thomas, E. L.; Cheng, S. Z. D. *Macromolecules* **2004**, *37*, 5292.
(18) Chen, W. Y.; Zheng, J. X.; Cheng, S. Z. D.; Li, C. Y.; Huang, P.; Zhu, L.; Xiong, H.; Ge, Q.; Guo, Y.; Quirk, R. P.; Lotz, B.; Deng, L.; Wu, C.; Thomas, E. L. *Phys. Rev. Lett.* **2004**, *93*, 028301−1.
(19) Taunton, H. J.; Toprakcioglu, C.; Fetters, L. J.; Klein, J. *Nature (London)* **1988**, *332*, 712.
(20) Granick, S.; Herz, J. *Macromolecules* **1985**, *18*, 460.
(21) Kent, M. S.; Lee, L. T.; Farnoux, B.; Rondelez, F. *Macromolecules* **1992**, *25*, 6240.
(22) Bhushan, B.; Israelachvili, J. N.; Landman, U. *Nature (London)* **1995**, *374*, 607.
(23) Milner, S. T. *Science* **1991**, *251*, 905.
(24) DiMarzio, E. A.; Guttman, C. M.; Hoffman, J. D. *Macromolecules* **1980**, *13*, 1194.
(25) Halperin, A.; Tirrell, M.; Lodge, T. P. *Adv. Polym. Sci.* **1992**, *100*, 31.
(26) Patel, S. S.; Tirrell, M. *Annu. Rev. Phys. Chem.* **1989**, *40*, 597.
(27) Mansky, P.; Liu, Y.; Huang, E.; Russell, T. P.; Hawker, C. J. *Science* **1997**, *275*, 1458.
(28) Prucker, O.; Naumann, C. A.; Ruhe, J.; Knoll, W.; Frank, C. W. *J. Am. Chem. Soc.* **1999**, *121*, 8766.
(29) Zhao, B.; Brittain, W. J. *Prog. Polym. Sci.* **2000**, *25*, 677.
(30) Ito, Y.; Ochiai, Y.; Park, Y. S.; Imanishi, Y. *J. Am. Chem. Soc.* **1997**, *119*, 1619.
(31) Prucker, O.; Rühe, J. *Macromolecules* **1998**, *31*, 592.
(32) Prucker, O.; Rühe, J. *Macromolecules* **1998**, *31*, 602.
(33) Kent, M. S. *Macromol. Rapid Commun.* **2000**, *21*, 243.
(34) Adamuti-Trache, M.; McMullen, W. E.; Douglas, J. F. *J. Chem. Phys.* **1996**, *105*, 4798.
(35) Carignano, M. A.; Szleifer, I. *Macromolecules* **1995**, *28*, 3197.
(36) Szleifer, I. *Curr. Opin. Colloid Interface Sci.* **1996**, *1*, 416.
(37) Fauré, M. C.; Bassereau, P.; Carignano, M. A.; Szleifer, I.; Gallot, Y.; Andelman, D. *Eur. Phys. J. B.* **1998**, *3*, 365.
(38) Alexander, S. *J. Phys. (Paris)* **1977**, *37*, 977.
(39) de Gennes, P. G. *Macromolecules* **1980**, *13*, 1069.
(40) Halperin, A. *Macromolecules* **1987**, *20*, 2943.
(41) Halperin, A. *J. Phys. (Paris)* **1988**, *49*, 131.
(42) Raphaël, E.; de Gennes, P. G. *Physica A* **1991**, *177*, 294.
(43) Milner, S. T.; Witten, T. A.; Cates, M. E. *Macromolecules* **1988**, *21*, 2610.
(44) Milner, S. T.; Wang, Z.-G.; Witten, T. A. *Macromolecules* **1989**, *22*, 489.
(45) Milner, S. T.; Witten, T. A.; Cates, M. E. *Macromolecules* **1989**, *22*, 853.
(46) Zhulina, E. B.; Borisov, O. V.; Brombacher, L. *Macromolecules* **1991**, *24*, 4679.

(47) Murat, M.; Grest, G. S. *Macromolecules* **1989**, *22*, 4054.
(48) Lai, P.-Y.; Binder, K. *J. Chem. Phys.* **1992**, *97*, 586.
(49) Grest, G. S.; Murat, M. *Macromolecules* **1993**, *26*, 3108.
(50) Wu, T.; Efimenko, K.; Genzer, J. *J. Am. Chem. Soc.* **2002**, *124*, 9394.
(51) For PEO-*b*-PS synthesis, see for example: Quirk, R. P.; Kim, J.; Kausch, C.; Chun, M. S. *Polym. Int.* **1996**, *39*, 3.
(52) For PLLA-*b*-PS synthesis, see: Guo, Y. Ph.D. Dissertation, Department of Polymer Science, The University of Akron, 2003.
(53) See for example: Wunderlich, B. *Macromolecular Physics*; Academic Press: New York, 1973; Vol. 1, Chapter 3.
(54) Unpublished results in our laboratory. It has been observed that below 60 °C the long period of semicrystalline PLLA homopolymer in small-angle X-ray scattering experiments disappears due to a small difference of electron densities between the crystalline and amorphous PLLA parts.
(55) Miyata, T.; Masuko, T. *Polymer* **1997**, *38*, 4003.
(56) De Santis, P.; Kovacs, A. J. *Biopolymers*, **1968**, *6*, 299.
(57) Hoogsteen, W.; Postema, A. R.; Pennings, A. J.; Ten Brinke, G.; Zugenmaier, P. *Macromolecules* **1990**, *23*, 634.
(58) Kobayashi, J.; Asahi, T.; Ichiki, M.; Okikawa, A.; Suzuki, H.; Watanabe, T.; Fukada, E.; Shikinami, Y. *J. Appl. Phys.* **1995**, *77*, 2957.
(59) Chen, J.; Cheng, S. Z. D.; Wu, S. S.; Lotz, B.; Wittmann, J.-C. *J. Polym. Sci., Polym. Phys. Ed.* **1995**, *33*, 1851.
(60) Kovacs, A. J.; Lotz, B.; Keller, A. *J. Macromol. Sci., Phys.* **1969**, *3*, 385.
(61) Cartier, L.; Okihara, T.; Lotz, B. *Macromolecules* **1997**, *30*, 6313.
(62) The R_g values of PS homopolymers were measured in Prof. Chi Wu's laboratory at Chinese University of Hong Kong. The PS samples were synthesized via anionic polymerization and possess the same MW's as the blocks in the diblock copolymers. In brief, the second virial coefficient data of a series of monodispersed PS homopolymers in the mixed (chlorobenzene/octane) solvent and amyl acetate were measured at different temperatures. The values of R_g^{PS} for the PS samples were estimated from hydrodynamic radius in these solutions. For PS chains, the mixed solvent is slightly better than the θ condition, while amyl acetate is a good solvent for PS chains which is about 6 times better than the mixed solvent.
(63) Lauritzen, J. I.; Hoffman, J. D. *J. Res. Natl. Bur. Stand.* **1960**, *64A*, 73.
(64) Hoffman, J. D.; Lauritzen, J. I. *J. Res. Natl. Bur. Stand.* **1961**, *65A*, 297.
(65) Wunderlich, B. *Macromolecular Physics*; Academic Press: New York, 1980; Vol. 3, Chapter 8.
(66) Hard-sphere-like model: for a real hard-sphere system, when $d \geq 2r$, free energy $G = 0$; when $d < 2r$, $G \rightarrow \infty$. There is a sharp transition of free energy at $d = 2r$ (or $\tilde{\sigma} \sim 1$). For our systems, the transition is also sharp, which is similar to the hard-sphere model. However, the polymer coils are not uncompressable hard spheres; they can penetrate into each other. At some point, therefore, the energy will not continue the sharp increase toward ∞, but rather slow down. After this "yield" point of the chains, when they start to overcrowd each other, the hard-sphere model is void.

MA052166W